

# Impact of spatial resolution on large-scale ice cover modelling of mountainous regions

Helen Werner<sup>1,2</sup>, Dirk Scherler<sup>1,3</sup>, Tancrede P. M. Leger<sup>4</sup>, Guillaume Jouvét<sup>4</sup>, Ricarda Winkelmann<sup>2,5,6</sup>

<sup>1</sup>Organic and Earth Surface Geochemistry, GFZ Helmholtz Centre for Geosciences, 14473 Potsdam, Germany

<sup>2</sup>Earth Resilience Science Unit, PIK Potsdam Institute for Climate Impact Research, 14473 Potsdam, Germany

<sup>3</sup>Institute of Geographical Sciences, Freie Universität Berlin, 12249 Berlin, Germany

<sup>4</sup>IDYST, Faculty of Geosciences and Environment, Université de Lausanne, CH-1015 Lausanne, Switzerland

<sup>5</sup>Institute of Physics and Astronomy, University of Potsdam, 14476 Potsdam, Germany

<sup>6</sup>Department of Integrative Earth System Science, Max Planck Institute of Geoanthropology, 07745 Jena, Germany

Correspondence to: Helen Werner (helen.werner@gfz.de)

**Abstract.** To compensate for the high computational costs when modelling large-scale mountain glaciers, ice fields or ice sheets over multiple millennia, it is common practice to coarsen the spatial resolution of numerical models to 1 km or more, which is not sufficient to describe complex valley topographies. Here, we examine the influence of spatial resolution by modelling a growing and retreating exemplary ice field in the European Alps at resolutions ranging from 50 m to 2 km using the Instructed Glacier Model (IGM). We find that while ice-covered areas remain similar, ice volume increases substantially with coarser resolution. Compared to the reference run at 50 m spatial resolution, model results at a resolution of 300 m and finer are comparable and sufficiently accurate to simulate topographically constrained ice flow. However, at resolutions coarser than ~800 m, topographic resampling artificially lowers slope angles and mountain peaks, providing a larger accumulation area at high altitudes, with thicker glaciers that are typically warm-based, while thinner glaciers at fine resolutions remain cold-based. Raised valley floors at coarse resolutions result in slower-flowing ice with increased thickness and glacial response times. The resulting hysteresis between climate forcing and glacial response at coarse resolutions is only partially decreased with slower temperature change. Seemingly stable model results at coarse resolutions may be misleading and accurate glacier geometries might arise from parameter choices that compensate for poorly resolved topography. Similar non-linear and altitudinal-dependent resolution effects are likely in mountain regions worldwide and emphasize the need for model advances to enable simulations at sufficiently high spatial resolutions to accurately resolve glacier dynamics.

## 1 Introduction

Mountain glaciers are a crucial component of the Earth's cryosphere, providing freshwater to approximately 1.9 billion people (Immerzeel et al., 2020). Anthropogenic climate change threatens these resources and simultaneously increases the risk of natural hazards in mountainous regions, such as ice-rock avalanches and glacier lake outburst floods (Hartmeyer et al., 2020; Huggel et al., 2019). On a global scale, glacier melt contributed to about 20 % of sea-level rise between 2000 and 2019 (Hugonnet et al., 2021). Over longer time scales, glaciers play an important role in shaping the landscape of many mountain ranges. In the European Alps, extensive glaciations carved steep and narrow peaks and formed over-deepened and U-shaped valleys during the Quaternary period (Ivy-Ochs, 2015; Liebl et al., 2021; Penck and Brückner, 1909). Studying past glaciations helps us to understand the future evolution of mountain glaciers under present-day climate change. Consequently, spatially distributed and accurate numerical models of mountain glaciers and ice fields are essential for both projecting future change and reconstructing former glaciations.

The horizontal resolution of numerical ice models has been shown to influence mass loss in simulations of continental-scale ice sheets and estimated sea-level contributions, particularly in regions with high bedrock elevation gradients (Cuzzzone et al., 2019; Rückamp et al., 2020; Williams et al., 2025; Aschwanden et al., 2016). In order to address resolution-related model inaccuracies, Williams et al. (2025) suggest resolutions of 5 km or finer for modelling regions in the West Antarctic ice sheet. For Greenland,

Cuzzone et al. (2019) propose a resolution of at least 10 km, Rückamp et al. (2020) report convergence of ISMIP6 (Ice Sheet Model Intercomparison Project; Nowicki et al., 2016) simulations at 1 km or finer, and Aschwanden et al. (2016) find that a resolution of ~600 m is required to model most Greenland outlet glaciers in best agreement with observational data. Resolution-related issues in ice sheet simulations may be efficiently mitigated using unstructured grids that refine the resolution in steep areas while keeping regions of more gentle sloping bedrock coarser (Cuzzone et al., 2019). However, for numerical models of mountain glaciers and ice fields, which are substantially controlled by the bedrock topography, resolution effects are expected to be stronger. Previous modelling studies of mountain-range scale glacier systems and ice fields in, e.g., the European Alps, the Tibetan Plateau, the Southern Alps of Zealand, typically used a km-scale resolution (e.g., Mey et al., 2016; Seguinot et al., 2018; Juvet et al., 2023; Golledge et al., 2012; Zhang et al., 2022), but a systematic analysis of the impact of grid resolution is lacking.

Alpine regions are characterized by a complex topography with high mountain peaks and narrow valleys connected by steep slopes. These topographical features influence the formation, dynamics, and mass balance of glaciers. For example, surface elevation controls the mass balance mainly through the temperature lapse-rate, whereas the steepness of the bed controls glacier flow. However, when resampling a digital elevation model (DEM) to a coarser resolution, some of the topographical details for peaks and valleys are lost due to spatial averaging (Fig. 1d, e). For example, with 4806 m a.s.l., the Mont Blanc, the highest peak of the European Alps, attains a height of 4745 m in a 100 m DEM, and only 4674 m when resampled to 1 km resolution. This leads to an overall loss of area at high altitudes in coarser-resolution DEMs (Fig. 1b). Similarly, steep slopes in high-relief mountain regions of typically 30° and more (e.g., Duncan et al., 2003; Korup et al., 2005) are reduced by resampling DEMs to coarser resolution, thereby changing first-order topographical characteristics. Specifically, at elevations higher than 1000 m a.s.l. in the Western Alps, average slope angles in a 100 m DEM are ~5–10° steeper compared to a 500 m DEM and even ~10–15° steeper compared to a 1000 m DEM (Fig. 1c). Coarse resolutions therefore fail to accurately represent the mountain topography that controls glacier dynamics.

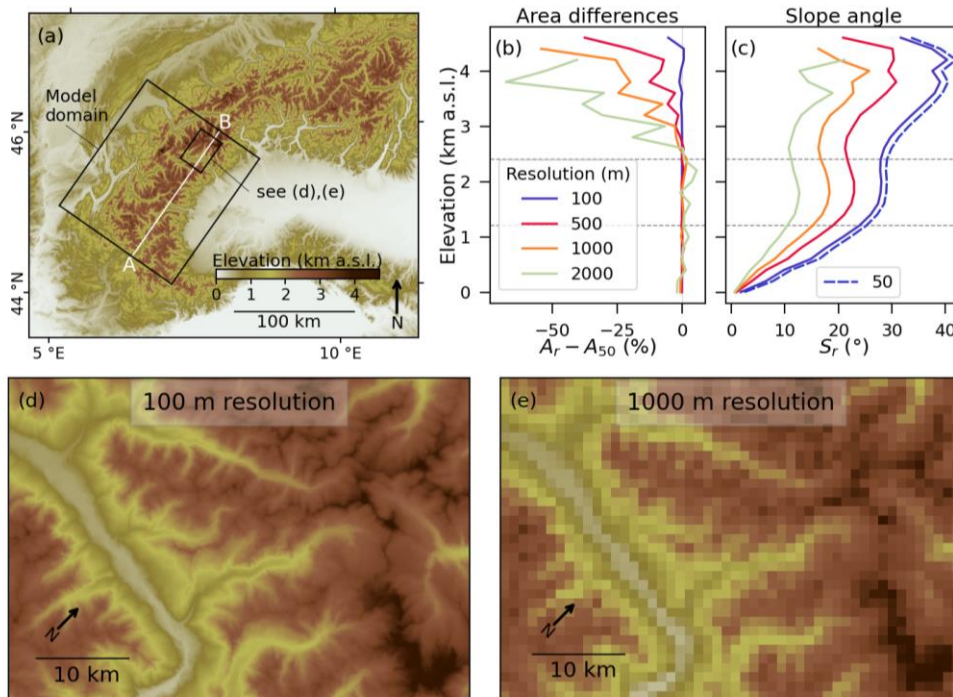


**Figure 1** Comparison of a digital elevation model (DEM) at different resolutions. (a) DEM of the Western Alps at 300 m resolution (cubically resampled from a 30 m resolution DEM from Tadono et al. [2014] with present-day glaciers and lakes removed using data from Cook et al., [2023]). Large rectangle indicates the model domain; small rectangle indicates subsets shown in (d) and (e). White line indicates transect between points A and B shown in Fig. 6. (b) Area differences between DEMs at different resolutions  $r$  ( $A_r$ ) and 50 m ( $A_{50}$ ) relative to the 50 m DEM as a function of elevation. Area corresponds to the Western Alps shown in (a) and differences are averaged in 200 m elevation bins defined by the 50 m DEM. (c) Slope angles of the Western Alps shown in (a) at different resolutions  $r$ , averaged in 200 m elevation bins defined by 50 m DEM.

Resolutions shown in (b) and (c) are 100 (blue), 500 (red), 1000 (orange), and 2000 m (grey); and 50 m in (c) (blue dashed). Dashed grey horizontal lines (b) and (c) at 1200 and 2400 m a.s.l. mark our defined thresholds for low (0–1200 m a.s.l.), mid (1200–2400 m a.s.l.), and high altitudes (<2400 m a.s.l.) shown in Figs. 4, 8, 9. DEMs of small rectangle subset shown in (a) at (d) 100 m and (e) at 1 km resolution.

To improve numerical models of former glaciations, they are calibrated with geological data, such as mapped and dated moraines or trimlines (e.g., Kamleitner et al., 2022; Wirsig et al., 2016; Mey et al., 2016). In the European Alps, comparisons between modelled ice surface elevations and trimlines suggest ice thickness overestimations during the Last Glacial Maximum (LGM, ~24,000 years ago) in models based on a km-scale resolution, e.g., by up to 1000 m in the Rhône Valley (Seguinot et al., 2018; Jouvét et al., 2023). A better match to trimline records was achieved by Mey et al. (2016) by adjusting the sliding coefficient in a steady-state model at 3 km resolution. Recent work by Leger et al. (2025) significantly reduced the Alps-wide mean mismatch between modelled ice surface elevations and trimlines to ~130 m in the best-scoring simulation of a 100-member ensemble by using a higher spatial resolution of 300 m. These results suggest that the agreement between numerical models and field data can be reduced not only through improved parameter choices but also by increasing the spatial resolution. However, it remains unclear whether even finer resolutions lead to more accurate results, and how spatial resolution influences other aspects of glacier modelling in alpine regions.

In this study, we explore the impact of spatial resolution on large-scale ice-cover modelling of a mountainous region. We employ the Instructed Glacier Model (IGM) to grow mountain glaciers up to an orogen-scale ice field over several millennia of model years, at different spatial resolutions ranging from 50 m to 2 km. Such computationally expensive experiments would be unfeasible with traditional glacier models, e.g., Elmer Ice (Gagliardini et al., 2013) or the Parallel Ice Sheet Model (PISM; Winkelmann et al., 2011). IGM enables us to overcome this computational bottleneck by using deep learning based on the higher-order Blatter-Pattyn model (Blatter, 1995). Although deviations between a full Stokes ice physics implementation and IGM are expected, our focus in this study is on the impact of spatial resolution on bedrock topography and ice model results, which we expect to be on the same order across different mechanical models. In the following, we first describe the glacier model and experimental design. Then, we present the model results, focusing on systematic differences across different spatial resolutions. Our analysis examines ice volume, thickness, velocity, and basal temperature in terms of their spatial and temporal variations. Finally, we discuss the underlying processes driving the spatiotemporal differences in ice cover and dynamics.

## 2 Methods and Materials

### 2.1 The Instructed Glacier Model (IGM)

IGM is an open-source Python model that simulates glacier evolution in 3D (Jouvét and Cordonnier, 2023). The ice flow model is based on physics-informed deep learning that achieves high computational efficiency - especially with Graphics Processing Units (GPU). Within run times of 9 days, we were able to apply IGM to our model domain at 50 m resolution with 16,150,000 pixels over a model time of 5000 years. Jouvét and Cordonnier (2023) showed that by directly enforcing physical laws in the learning process, IGM reproduces the solutions of a high-order analytical solver of ice flow with high fidelity. The physics-informed deep learning approach is independent of training data from other glacier models, which allows us to run the same experimental setup at different spatial resolutions and directly compare the model results. A direct comparison of a simulation of the European Alps at 2 km resolution using IGM to the respective simulation using the well-tested and widely used Parallel Ice Sheet Model (PISM; Winkelmann et al., 2011) published by Jouvét et al. (2023) showed minor deviations, confirming that the alpine ice field is a suitable application for IGM (Leger et al., 2025). Our setup is based on Leger et al. (2025), where IGM was used to produce a model of the LGM in the Alps that closely matches geological evidence. We used the parameterisation from Leger et al. (2025)'s best-scoring simulation (number 37) out of an ensemble of 100 Alps-wide simulations at 300 m resolution. This setup is therefore well-adopted

to the Alps and the formation of an extensive ice field. In the following, we briefly describe the submodules covering essential glacier processes. All model parameters can be found in the supplements (Table S1).

The ice flow module in IGM is designed to efficiently simulate 3D velocities using a physics-informed deep learning approach. Instead of solving costly Stokes equations or approximations thereof, ice velocities are simulated by an inexpensive convolutional neural network (CNN) (for a detailed description see Jouvét and Cordonnier, 2023). The ice velocities are simulated as energy-minimizing solutions of the higher-order Blatter-Pattyn model (Blatter, 1995) which has been shown to reproduce ice velocities that agree well with full Stokes models (Pattyn et al., 2008). The generic emulator is capable of handling a variety of ice flow and temperature regimes which is important for modelling alpine ice fields since mountain glaciers exhibit a range of flow velocities (Millan et al., 2022; Jouvét and Cordonnier, 2023). Ice flow at the ice-bedrock boundary is described by a non-linear Weertman friction condition (e.g., Schoof and Hewitt, 2013) with an exponent of four. The initial glacial state is based on a pretrained CNN described in Jouvét and Cordonnier (2023) to advance convergence to the Blatter-Pattyn model in the first time steps. For this pretraining, the emulator was trained over a diverse catalogue of glaciers and flow regimes at 100 m spatial resolution with 10 vertical layers, fine vertical discretization close to the ice-bedrock interface, 16 CNN-layers, and 32 CNN-output filters (Jouvét and Cordonnier, 2023). For adjustments to new ice field states attained through run time, we retrained the physics-informed neural network multiple times within a single model year (every  $\sim 0.18$  years). The on-the-fly retraining in the highest-resolution simulations at 50 and 100 m was performed more often (every  $\sim 0.05$  years) to resolve the more complex topography with its steeper slopes at finer resolutions (Fig. 1). The retraining frequencies were found to be high enough to ensure that the emulator's deviation from the analytical solver typically remains below  $5 \text{ m yr}^{-1}$  in ice velocity for test cases on the Aletsch and LGM-Rhône glaciers (see Figs. 4–7 in Jouvét and Cordonnier, 2023). Computations at 50 and 100 m resolutions were executed on a  $\sim 7000$ -core Nvidia A100 GPU, for coarser resolutions we used a Nvidia A40 and A30 GPU.

The enthalpy module follows an energy-conservative formulation by Aschwanden et al. (2012). It distinguishes between cold and temperate ice: For cold ice at temperatures below the pressure-melting point, enthalpy is proportional to pressure-adjusted temperature, while for temperate ice, enthalpy includes an additional component incorporating the creation of water content through energy transfer. The Arrhenius factor in the Blatter-Pattyn model for ice flow depends on the pressure-adjusted ice temperature and is calculated via the Glen-Paterson-Budd-Lliboutry-Duval law (Cuffey and Paterson, 2010). The sliding coefficient follows the Mohr-Coulomb sliding law (Cuffey and Paterson, 2010) and accounts for basalt melt and meltwater production when the pressure melting point is reached. At the ice surface, enthalpy is constrained by surface temperature, which is modified by our temperature forcing (see Sect. 2.2). At the glacier bed, boundary conditions depend on the temperature at the bottom ice layer and bed surface, where we set the geothermal heat flux to  $0.065 \text{ W m}^{-2}$  across the entire model domain, which is in the range of reported values in the European Alps (Goutorbe et al., 2011).

The surface mass balance (SMB) computation is based on a temperature-index model (e.g., Hock, 2003) to calculate the SMB from monthly near-surface air temperature and precipitation. Ice surface accumulation is equal to precipitation when air temperatures are below  $0 \text{ }^{\circ}\text{C}$  and decreases to zero linearly with temperatures between  $0$  and  $2 \text{ }^{\circ}\text{C}$ . Ablation is computed with a positive-degree-day model using the integral formulation from Calov and Greve (2005) that accounts for stochastic temperature variations. To prevent ice flow beyond our model domain, we set the SMB to  $-50 \text{ m yr}^{-1}$  at a distance of 5 km from the model domain edges.

Modelling space- and time-dependent bed deflection as a response to ice loading and unloading is realized by coupling IGM with the gFlex model (Wickert, 2015) using the two-dimensional elastic thin-plate equation in Mey et al. (2016). Based on Leger et al.

150 (2025)'s best-scoring ensemble simulation, we assume a lithospheric effective elastic thickness of 45 km and set the frequency of gFlex iterations to 50 years with a spatial resolution of 2 km.

Avalanching impacts ice accumulation, surface elevation, as well as flow velocity and is especially relevant for modelling ice fields at high resolution where slopes are generally steeper (Fig. 1c). The avalanche module in IGM is based on Kessler et al. (2006) and 155 redistributes modelled accumulation downslope until the glacier surface reaches an angle of repose, here set at 45 °. This process is applied at a frequency of five years.

## 2.2 Experiment design

As we aim to investigate resolution-related ice model differences in mountainous regions, we chose a region with a complex alpine topography featuring high mountain summits as well as deep and narrow valleys. The ice field we modelled is located in the Western 160 Alps, encompassing several mountain massifs with elevations exceeding 4000 m a.s.l. (Fig. 1a). This mountainous region provides the glacier bed for a system of small tributary glaciers, which flow over steep terrain with an average slope of 21.5 ° and eventually merge into large and thick valley glaciers (>5 km wide, up to ~100 km long). Our model domain is positioned near the southwestern end of the European Alps, where it is naturally bounded by lowlands to the northwest and southeast. To enhance computational efficiency, we rotated the model domain clockwise by 55° to reduce the number of lowland pixels that do not contribute to the ice 165 cover, constraining the model area to a total of 40,375 km<sup>2</sup> (Fig. 1a). Our modelled ice field on this topography covers a maximum area of ~12,700 km<sup>2</sup>, comparable in size to the present-day Southern Patagonian Icefield (~12,200 km<sup>2</sup>; Meier et al., 2018). The bedrock topography is taken from the ALOS World 3D 30 m DEM (Tadono et al., 2014), which was resampled to 50 m with present-day glaciers and lakes removed based on Cook et al. (2023). The DEM is resampled to multiples of 100 m resolution between 100 and 1000 m and multiples of 200 m up to 2000 m. For all DEM resampling of input fields, we use cubic convolution due to its 170 higher accuracy in resolving surface elevation and slope angles compared to other resampling methods like bilinear or kriging interpolation (Minh et al., 2024). In all experiments the resolution in the x- and y-directions is equal. Every simulation starts with ice-free conditions.

We used a simplified climate setup as we aimed to assess the influence of spatial resolution on a growing and melting ice field 175 instead of reconstructing past glaciations. We applied a synthetic temperature forcing that mimics transient cooling and warming within the range of temperature rates that occurred during the last glacial cycle (Jouzel and Masson-Delmotte, 2007), allowing for the build-up of a large ice field like during the LGM. The forcing begins with an initialization phase of 1000 years with no temperature change to ensure that the initial glacial state is in balance with our setup. The initialization phase is followed by linear cooling over 2000 years down to -8 K relative to the starting condition and a warming phase over another 2000 years until the entire 180 cooling is reversed. The cooling and warming rates are -4 and +4 K per 1000 years, respectively, and the total model time is 5000 years. We carried out additional experiments with a slower temperature cooling and warming of -2 and +2 K per 1000 years stretched out over 4000 year-long cooling and warming phases, resulting in a total model time of 9000 years. These simulations were run at 100, 500, and 1000 m spatial resolution. All simulations started with temperature and precipitation conditions similar to the present-day. Monthly temperature and precipitation values are derived from climate data averaged over 1981–2010 from a 185 weather station in Modane, France, located at 1228 m a.s.l. within the model domain (Météo-France, 2022). We used a lapse-rate of 6 °C per 1000 m elevation to project the temperatures across the entire model domain. The resulting mean annual temperature at sea level is ~14.9 °C. With an annual sum of 0.66 m w.e. (meter water equivalent), the weather station's precipitation values lie at the lower end of typical values in the European Alps (e.g., Isotta et al., 2014). Therefore, to ensure that the ice field covers the entire mountainous part of the model domain at the time of maximum cooling, we multiplied monthly precipitation values by 1.6, resulting

190 in a more realistic annual precipitation of 1.06 m w.e. per year. Those monthly precipitation values were kept constant in space and unchanged throughout the warming and cooling phases.

### 2.3 Model output analysis

To compare simulations across all resolutions, we resampled all model inputs and outputs to 50 m using nearest-neighbour interpolation to preserve the pixel structure while avoiding artefacts from coarse-resolution resampling. We analysed differences relative to the highest-resolution simulation at 50 m, which serves as our reference. Spatially distributed model results are analyzed within a defined mask that is based on glacial drainage basins located well-inside the model domain at maximum ice coverage of the 50 m simulation. We thus excluded any glacier catchments that lead to ice flow reaching the domain borders to avoid biases in results from our non-mass-conserving domain boundary scheme of ice melt. We used elevation bands of 0–1200 m, 1200–2400 m, and >2400 m a.s.l. to distinguish between different altitudes that correspond to deeply incised, gently sloping valleys at low altitudes and steep mountain summits at high altitudes, and a transitional domain, where much of the modelled ice volume is located (Fig. 1c). A map showing the distribution of the elevation bands across the model domain can be found in the supplements (Fig. S1). For the purpose of this study, we introduce the notation  $X_r$  for any input or output variable  $X$  at resolution  $r$  (in metres) and denote bedrock elevation with respect to mean sea level.

## 3 Results

### 205 3.1 Topographic variability of resampling effects

The changes in surface elevation due to resampling the 50 m DEM to a coarser resolution are not uniform across the landscapes. Based on the notion that resampling to a coarser resolution affects large and deep valleys less compared to small tributary gorges or ravines, we assessed elevation differences for valleys of distinct Strahler stream order (Strahler, 1957), using a minimum upstream area of 0.5 km<sup>2</sup>. The Strahler order defines the stream size based on a hierarchy of tributary streams. Streams of order 1 are the smallest without any tributaries. As the Strahler order increases, the streams and associated valleys have more branches upstream, their upstream area increase and so does the discharge and size of the valley (see Fig. S2). Elevation differences between variously resampled DEMs and the reference DEM at 50 m resolution vary with Strahler order, with the highest discrepancies at intermediate Strahler orders (3–4) (Fig. 2). At these Strahler order, median elevation difference values range from 150 to over 250 m for DEMs resampled to a resolution of 1000 m and coarser compared to the 50 m DEM. In contrast, at very low (1) or high (6–7) Strahler orders, corresponding to small and steep as well as large and gentle valleys, respectively, median elevation difference values are less than 165 m, for any resolution. At streams of low order, bedrock elevation tends to be higher than in the 50 m DEM, though differences extend to more negative values than at any higher stream order. Elevation differences in large valleys of high streams orders (6–7) are small and strictly positive, resulting from resampling-induced elevated valley floors. At 300 m resolution and finer, resampling effects are small and median values remain below 50 m, regardless of the stream order. Overall, resampling effects at resolutions of 1000 m and coarser are strong, especially in intermediate valleys, while effects at fine resolutions and in large valleys are minor.

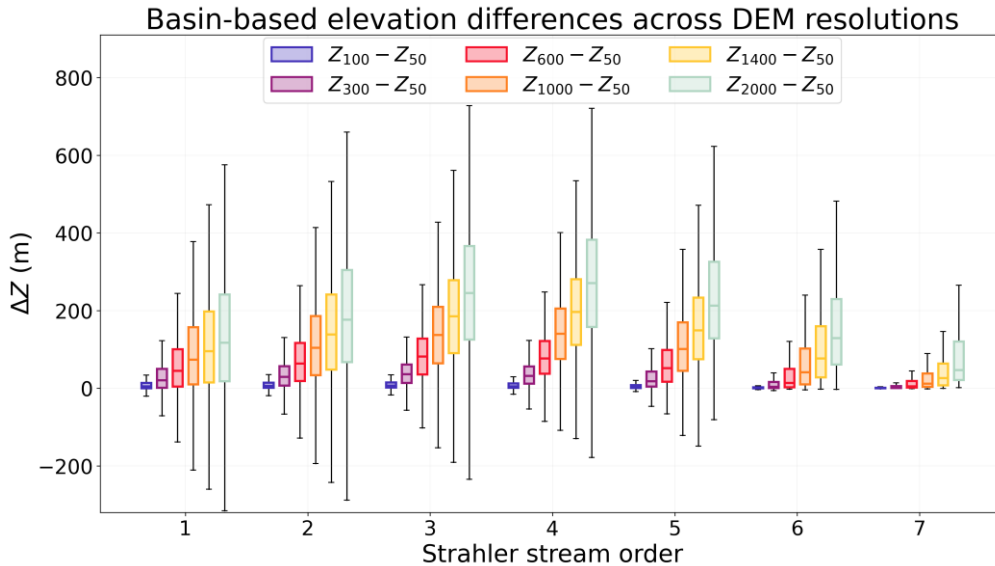
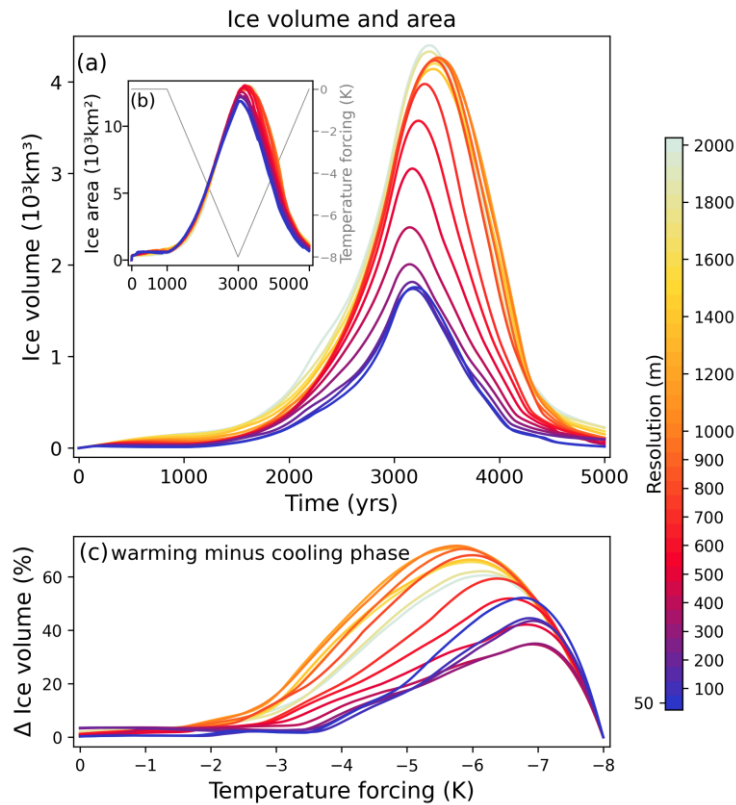


**Figure 2** Elevation differences  $\Delta Z = Z_r - Z_{50}$  in the Western Alps (see extent in Fig. 1a) between the 50 m DEM and DEMs at resolutions of  $r = 100$  (blue), 300 (purple), 600 (red), 1000 (orange), 1400 (yellow), and 2000 m (grey) by valley type defined by Strahler order (Strahler, 1957). Boxes extend from the first quartile to third quartile with a line at the median. The whiskers extend from the box to the farthest data point lying within 1.5 times the interquartile range from the box.

### 3.2 Temporal evolution of ice volume and area

Over the entire model duration, a coarser spatial resolution leads to an increase in ice volume, despite similar ice extents (Fig. 3a, b). After the initialization phase (0–1000 years), the 2000 m simulation has  $\sim 160 \text{ km}^3$  of ice volume, which is more than 10 times that of the 50 m run ( $\sim 12 \text{ km}^3$ ). Maximum ice volumes at 300 m resolution and finer are comparable, and increase steadily at intermediate resolutions (Figs. 3a, S3). At resolutions coarser than 800 m, maximum volumes are consistently high, exceeding  $40,000 \text{ km}^3$  and culminating in a factor  $\sim 2.5$  difference between the 50 and 2000 m simulations. In contrast, maximum ice area values range only slightly between  $11,900$  and  $13,000 \text{ km}^2$ .

Hysteresis between modelled ice volume and temperature forcing increases at coarser resolutions. In all simulations, the timing of maximum ice volume lags behind the strongest cooling of  $-8 \text{ K}$  at 3000 years. However, the delay of peak ice volume is most pronounced at resolutions coarser than 800 m, with a time lag of up to 420 years compared to a delay of less than 200 years at 300 m resolution and finer (Figs. 3, S3). Time lags in reaching the maximum ice area are much smaller than for ice volume, yet still increase with coarser resolution. Larger and persistent volume differences between the warming (3000–5000 years) and cooling phases (1000–3000 years) occur in the coarse resolution simulations for temperature forcings stronger than  $-3 \text{ K}$  and thus during large parts of the model run (years  $\sim 1750$ – $4250$ ) (Fig. 3c). At resolutions coarser than 800 m, ice volumes during the warming phase are more than 60 % higher than during the cooling phase under the same temperature forcing, relative to the maximum ice volume. Overall, we find that fine resolutions capture temperature-driven changes more accurately, indicated by shorter delays in reaching the maximum ice volume as well as smaller differences between the warming and cooling phases.



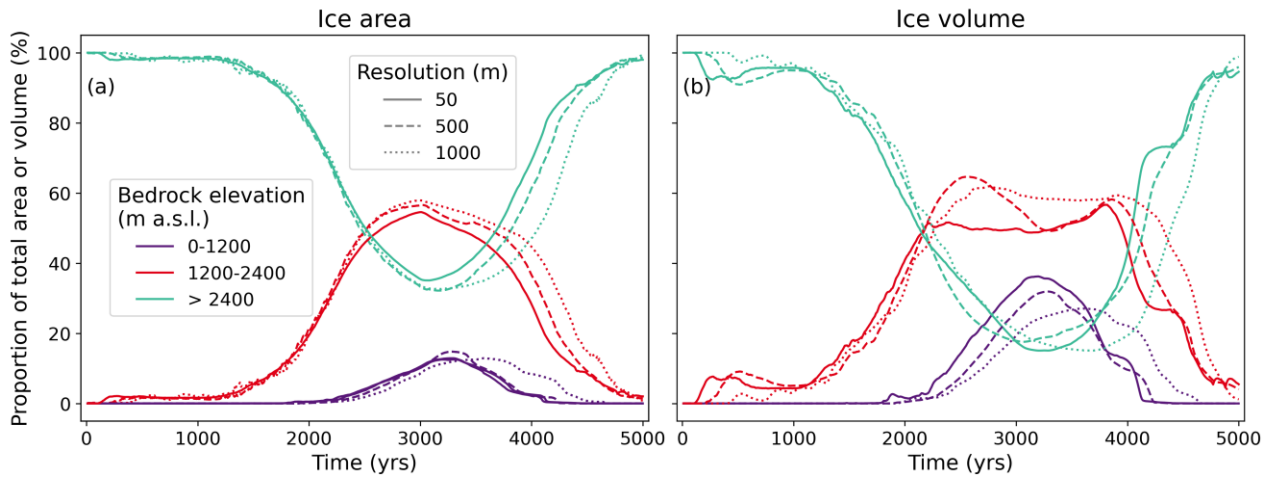
245

**Figure 3** Temporal evolution of (a) ice volume and (b) ice area at resolutions between 50 and 2000 m. The temperature forcing is shown in (b) (grey). (c) Ice volume differences at times with the same temperature forcing value during the warming (3000–5000 years) and cooling phase (1000–3000 years) (warming minus cooling phase) relative to the maximum ice volume in each run. For example, a temperature forcing of -4 K is applied at model year 2000 (cooling phase) and again at year 4000 (warming phase). The relative ice volume difference at -4 K is computed as the difference in ice volume at years 4000 and 2000 relative to the maximum ice volume at each resolution.

250

Resampling effects on the DEMs related to valley size (Fig. 2) only partly coincide with changes in ice volume proportions across bedrock altitude (Fig. 4). The distribution of ice volume as well as timing of its maximum is significantly influenced by resolution at mid (1200–2400 m a.s.l.) and low altitudes (0–1200 m a.s.l.). In contrast, at high altitudes (>2400 m a.s.l.) with drainages of generally low Strahler order, resolution-related differences in the topography and ice volume are small (Figs. 2, 4). At around 2000–2500 years, thick glaciers begin to form in large valleys, causing low altitudes to contain more ice volume than high altitudes, although covering less ice area. While resampling effects are minor in large valleys located at low altitudes (Fig. 2), resolution effects on the distribution of ice volume are most pronounced there: Ice volume at low altitudes grows relatively slower and contributes less to total ice volume at coarser resolutions (Fig. 4b). At 1000 m resolution, the maximum share of low-altitude ice volume is about 10 % less than at 50 m resolution. This reduced contribution is compensated for by mid altitudes, which contain relatively more volume in the coarse than in the fine resolution simulation. The time lag between maximum cooling and the onset of ice melt are observed at all altitudes but originates from low altitudes, where ice volume and area contributions decrease ~500 years later in the 1000 than in the 50 m simulation. In contrast, for ice area, resolution effects are overall small and rather independent of altitude (Fig. 4a).

260



265

**Figure 4** Temporal evolution of the contribution of low (0–1200 m a.s.l., purple), mid (1200–2400 m a.s.l., red), and high (> 2400 m a.s.l., green) bedrock altitudes to (a) total ice-covered area and (b) total ice volume. Results are shown for simulations at 50 (solid lines), 500 (dashed lines), and 1000 m (dotted lines) resolution and bedrock altitude is defined with respect to the DEMs at the corresponding resolution.

### 3.3 Ice field conditions at full glaciation

270

The ice volume deviations that depend on resolution and altitude (Figs. 3, 4) arise from spatially non-uniform ice thickness patterns. At full glaciation, ice thickness maps differences relative to the 50 m reference run reveal distinct spatial patterns between fine and coarse resolutions (Fig. 5; full version in Fig. S4). For comparison, maps of absolute ice thickness are shown in the supplement (Fig. S5). Among resolutions of 300 m and finer, ice thickness is generally comparable, and differences only increase slightly with coarser resolution (Fig. 5a, b). At these resolutions, large valley glaciers are marginally thicker, while small tributary glaciers are slightly thinner than in the 50 m simulation. Differences in ice thickness among the fine resolutions mostly remain below 100 m,

275

except at some glacier termini, where they are related to different extents. For coarser resolutions, ice thickness differences increase significantly and are generally positive (Fig. 5c–f). Although the main valleys are less affected by resampling (Fig. 2), the glaciers filling these valleys are most affected by coarser resolution, with thickness differences reaching a few hundreds of meters. Negative differences are exceptions and restricted to glacier termini. At the coarsest resolutions, the spatial pattern of high thickness differences in major valleys is less pronounced and negative differences appear more often (Fig. 5f). This indicates that, considering

280

each individual pixel, ice thickness differences do not increase monotonically between 50 and 2000 m resolution.

### Ice thickness differences at maximum ice volume

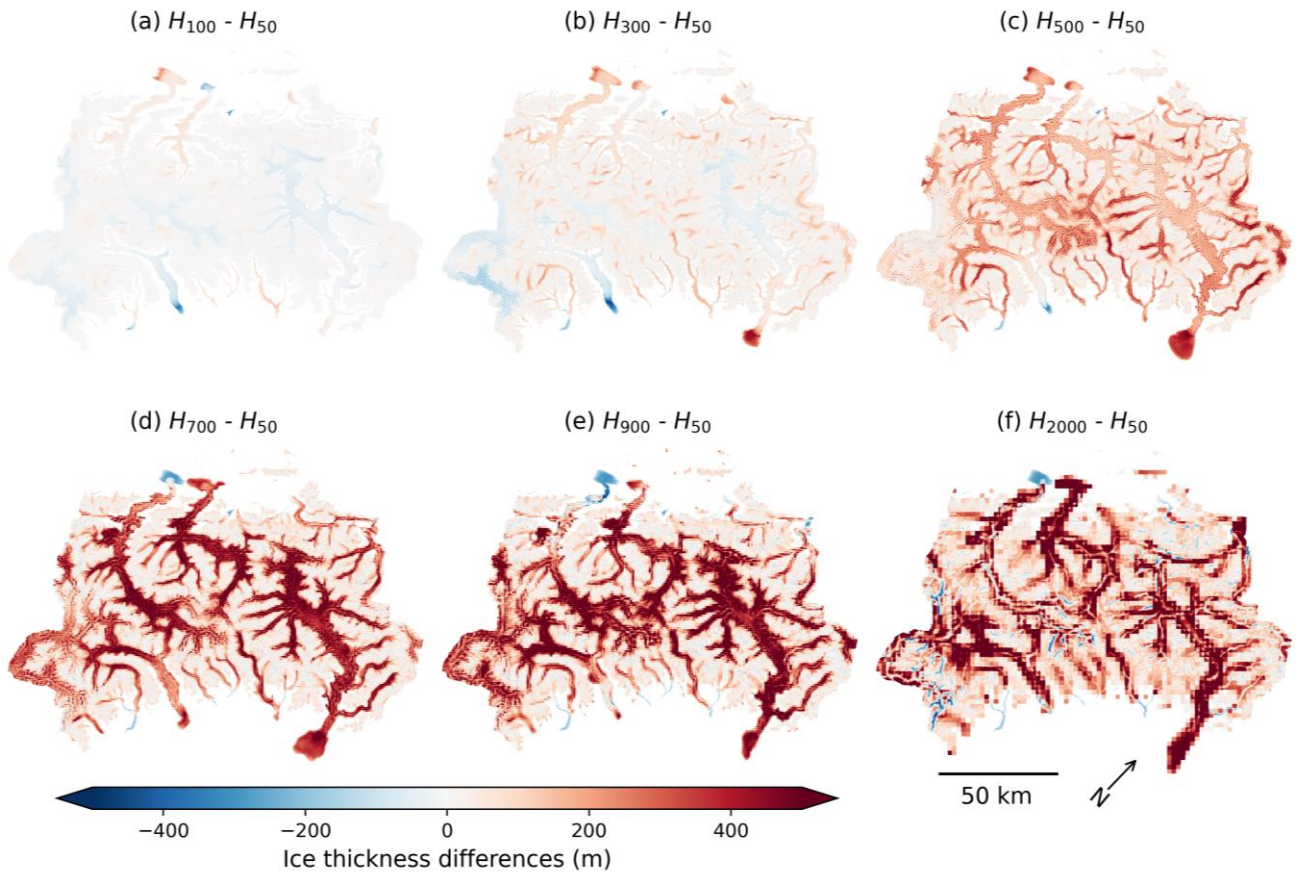
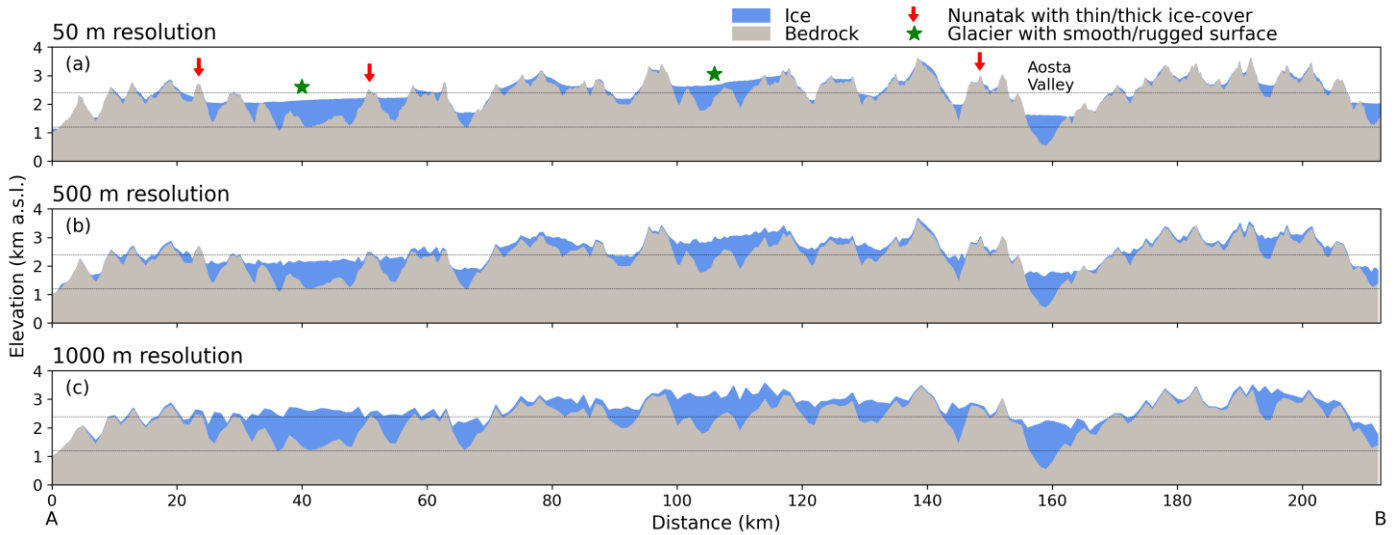


**Figure 5** Ice thickness differences ( $\Delta H = H_r - H_{50}$ ) between simulations at resolution  $r = 100, 300, 500, 700, 900, 2000$  m and the 50 m reference run, each at the time step of maximum ice volume. Blue colours indicate thicker ice in the 50 m run; red colours indicate thicker ice at the coarser resolution  $r$ .

A visualization of ice thickness with underlying bedrock along a transect reveals resolution-related differences in smaller-scale features of ice surface elevation (Fig. 6). At fine resolution, thick glaciers show smooth surfaces, even though the underlying bed is rough (Fig. 6a). However, at coarser resolutions, the ice surface is rugged with larger variations in ice thickness, despite overall thicker ice. This unrealistic imprint of bedrock topography in the ice surface increases with coarser resolution. The highest mountains are covered by relatively thin ice in all simulations. However, while ice thickness on nunataks (exposed summits surrounded by ice) is typically  $\sim 5$  m in the 50 m run, it increases to more than 100 m in the simulation at 1000 m resolution (Fig. 6). Large valleys such as the Aosta Valley are filled with thicker ice at coarser resolutions, allowing the ice to reach higher elevations. As a result, the Aosta Valley glacier in the transect is connected to tributary glaciers from the valley sides at 1000 m resolution that are absent in the 50 m run (Fig. 6).



295

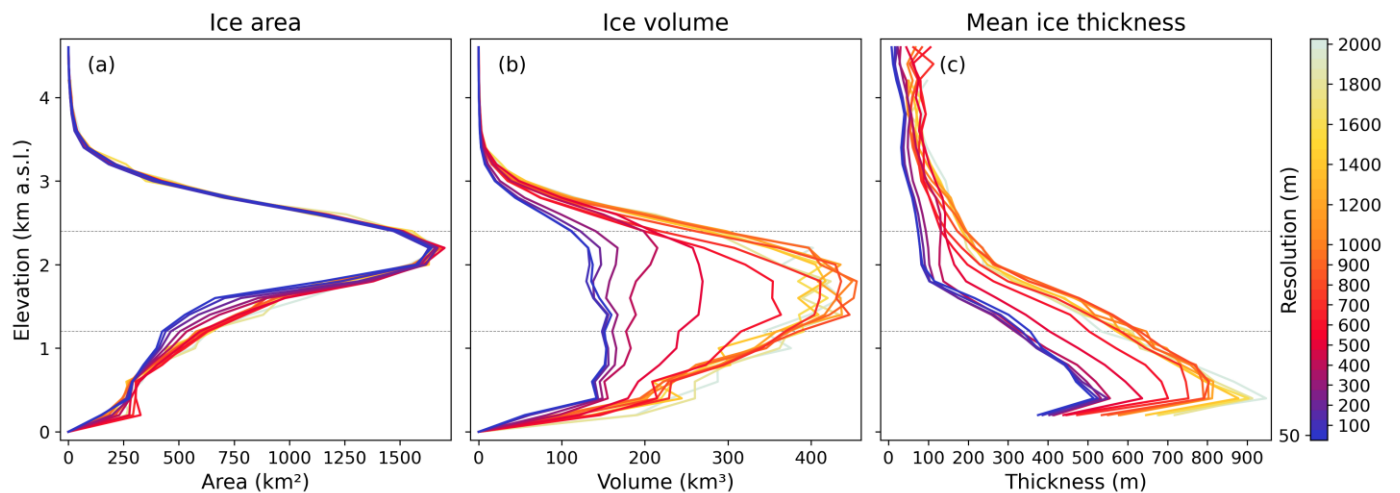
**Figure 6** Bedrock (grey) and ice thickness (blue) at the time of maximum ice volume across the transect between points A and B shown in Fig. 1a at (a) 50, (b) 500, and (c) 1000 m resolution. Red arrows mark exemplary nunataks with thin ice in the 50 m resolution run and high ice thickness at coarser resolution. Glaciers marked with green stars are smooth in the 50 m run but rugged at coarser resolution. Vertical lines at 1200 and 2400 m a.s.l. mark our defined thresholds for low (0–1200 m a.s.l.), mid (1200–2400 m a.s.l.), and high altitudes (>2400 m a.s.l.) in Figs. 4, 8, and 9.

300

A closer look at the distribution of ice across bedrock elevations shows how thickness and area influence ice volume at different spatial resolutions (Fig. 7). Most of the ice field’s area is located at ~2200 m a.s.l. irrespective of resolution, dropping off quickly with lower elevation (Fig. 7a). However, because the mean ice thickness simultaneously increases with lower elevations in all simulations, the ice volume attains maximum values at mid altitudes. The elevation range for high ice volume spans ~500–2200 m a.s.l. at fine resolutions, but it is more focused in the range ~1300–2200 m a.s.l. at resolutions coarser than 800 m (Fig. 7b). This shift is largely due to the general thickening of the glaciers in coarser resolution models (Fig. 7c). Whereas resolutions of ~300 m and finer produce mean thickness of similar magnitude and distributions across bedrock altitudes, resolutions coarser than ~800 m show much higher thickness that are comparable among these coarse resolutions, with large changes at intermediate resolutions (Fig. 7c). At ~1500 m a.s.l., increased ice thickness and area lead to over 160 % more ice volume at resolutions coarser than 800 m compared to the 50 m run. The strong increase in ice volume at mid altitudes is unmatched at other elevations and reflects the relative redistribution from low to mid altitudes at coarse resolutions, already indicated in Fig. 4. At low elevations of ~500 m a.s.l., the mean thickness of large valley glaciers increases significantly with coarser resolutions. However, these differences play a minor role in the total ice volume changes due to the limited number of large valley glaciers.

305

310



315

**Figure 7** (a) Ice area, (b) ice volume, and (c) mean ice thickness across bedrock elevation for simulations at resolution  $r$ . All values are calculated at the time of maximum ice volume for each run, and with respect to 200 m elevation bins of the corresponding DEMs at resolution  $r$ . Dashed

horizontal lines in grey at 1200 and 2400 m a.s.l. mark our defined thresholds for low (0–1200 m a.s.l.), mid (1200–2400 m a.s.l.), and high altitudes (<2400 m a.s.l.) in Figs. 4, 8, and 9.

Non-linear resolution effects are observed for various variables that describe the mean state and dynamics of the ice field (Fig. 8).

320 The magnitude of these changes varies with bedrock altitude, as already seen for ice thickness and volume (Figs. 5, 7). Despite non-linear changes in model outputs, differences in input DEM elevation and slope compared to the 50 m reference run vary monotonically with resolution and are negligible for fine resolutions up to 300 m (Fig. 8a, b). Modelled ice volume and mean thickness at maximum glaciation are comparable at fine resolutions but increase strongly at intermediate resolutions before levelling off at coarse resolutions. This pattern is most distinct at mid and low altitudes (Fig. 8c, d). The particularly strong increase in ice  
325 volume at mid altitudes (Fig. 8c) originates from large differences in mean ice thickness that integrate over a large glacial area, as shown in Fig. 7.

Apart from geometrical differences, we also observe non-linear resolution-related changes in the ice field's dynamics, with generally slower flow velocities at coarser resolution (Fig. 8e). Average velocity differences at low and mid altitudes are small at the finest  
330 resolutions and most pronounced at resolutions between 400 and 800 m, with substantial reduction in ice velocities. For instance, at low altitudes, where glaciers flow fastest, mean velocity values drop from over 200 m yr<sup>-1</sup> at 500 m resolution to less than 150 m yr<sup>-1</sup> at resolutions coarser than 800 m. At these altitudes, average values increase slightly among resolutions of 300 m and finer, which is noteworthy because an increase in average velocities with coarser resolution is only observed at these altitudes.

335 Finally, resolution-related changes in the thermal regimes are most pronounced at high altitudes (Fig. 8f). Average ice temperatures at the glacier base transition from cold-based (-4.8 °C at 50 and 100 m resolution) to temperate conditions at resolutions coarser than 1000 m. Similarly, at mid altitudes mean basal temperatures shift from ~-0.8 °C at fine resolutions to 0 °C at 800 m resolution, while ice at the base generally remains temperate at low altitudes across all resolutions. Overall, ice field characteristics during full  
340 glaciation shift from relatively thin and fast-flowing glaciers at fine resolutions (~50–300 m) to thick, slow flowing and generally temperate ice at coarse resolution (~800–2000 m).

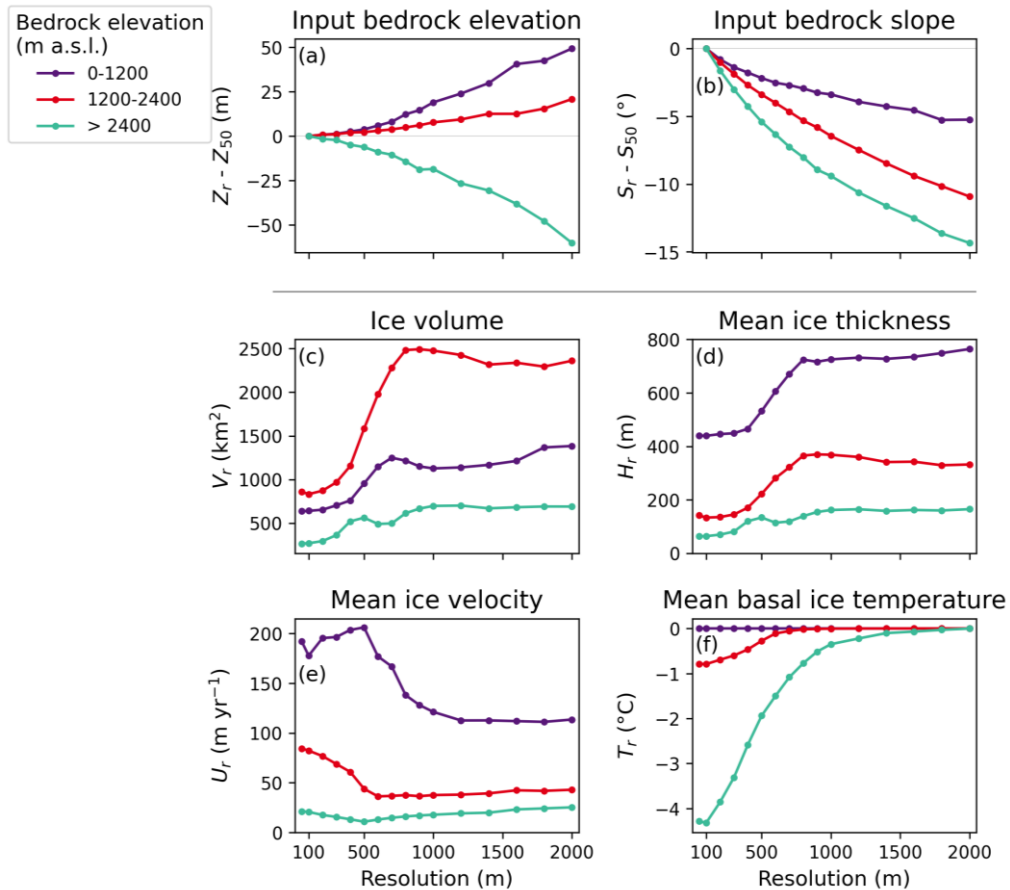


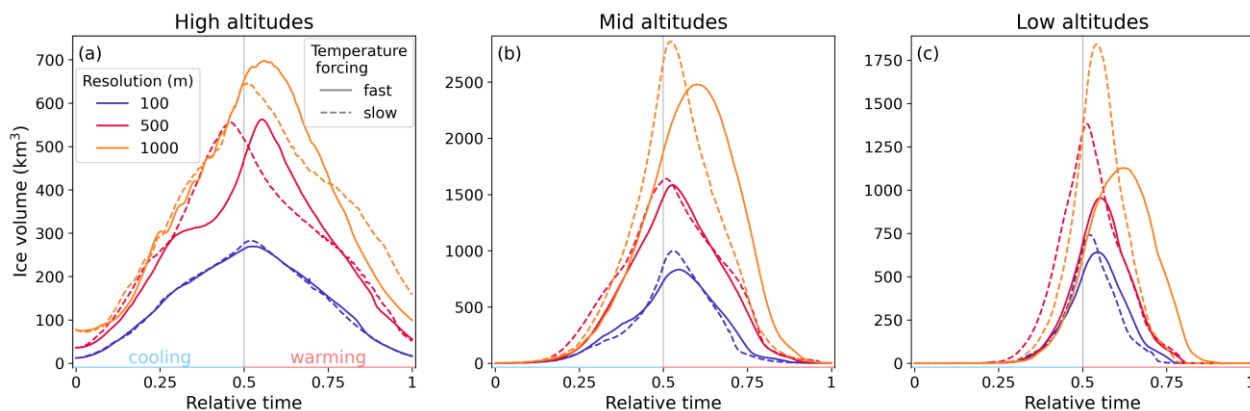
**Figure 8** Comparison of model inputs and outputs at low, (0–1200 m a.s.l., purple), mid, (1200–2400 m a.s.l., red), and high altitudes (> 2400 m a.s.l., green). Mean differences of (a) bedrock elevation ( $\Delta Z = Z_r - Z_{50}$ ) and (b) bedrock slope ( $\Delta S = S_r - S_{50}$ ) of the input DEMs at resolution  $r$  compared to the 50 m DEM. All means in (a) and (b) are taken over the glaciated area at 50 m and resolution  $r$ , and bedrock altitudes are defined with respect to the 50 m DEM. Model output variables are shown in (c)–(f) and refer to the time of maximum ice volume in each simulation at resolution  $r$ : (c) ice volume ( $V_r$ ), (d) mean ice thickness ( $H_r$ ), (e) mean depth-averaged ice velocity ( $U_r$ ), (f) mean pressure-adjusted basal ice temperature ( $T_r$ ). All means in (c)–(f) are taken over the glaciated area at resolution  $r$  and bedrock altitudes are defined with respect to the DEM at resolution  $r$ .

### 3.4 Impact of temperature forcing rate

A comparison of modelled ice volume under fast ( $\pm 4$  K/kyr) and slow ( $\pm 2$  K/kyr) temperature forcing shows that different cooling rates strongly affect coarser resolution results, while results at fine resolutions are rather comparable (Fig. 9). The maximum ice volume increases with the slow compared to the fast temperature forcing for all resolutions. This increase is most pronounced at coarse resolutions, with  $\sim 25\%$  more ice volume using the slow cooling rate in the 1000 m resolution run, whereas the increase is only 12% at 100 m resolution. Most of the added ice volume originates from low altitudes (Fig. 9c). However, ice volume differences related to spatial resolution are more pronounced than those caused by the change in temperature forcing rate. In particular, the peak ice volume more than doubles between the 50 and 2000 m simulations, with 138% more volume under fast and 162% under slow forcing.

Despite these differences, the distribution of ice volume across altitude bands remains largely unchanged and most of the ice volume is contained at mid altitudes in all simulations (Fig. 9b). The shift of ice volume distribution from low to mid altitudes with coarser resolutions at full glaciation (Fig. 4) is persistent under slower temperature forcing but reduced from 10% to  $\sim 5\%$  with fast temperature forcing. Under both temperature forcings, ice volume at high altitudes changes more gradually, while low-altitude regions respond with abrupt and strong increases and decreases. The delay in reaching the maximum ice volume with respect to temperature forcing is reduced with the slower temperature change: In the 1000 m runs, the lag drops from 420 to 250 years, driven

365 by continued ice growth at low altitudes, while glaciers at mid and high altitudes are more sensitive to temperature change and start to retreat earlier. In comparison, the maximum ice volume in the 100 m run is reached only  $\sim 200$  years after the peak cooling under both forcings. Reduced hysteresis effects are also apparent in lower volume differences between the warming and cooling phases using the slower forcing, especially at coarse resolutions (Fig. S7).



370 **Figure 9** Ice volume under fast ( $\pm 4$  K/kyr, solid line) and slow ( $\pm 2$  K/kyr, dashed line) temperature forcing at 100 (blue), 500 (red), and 1000 m  
 (orange) resolution at (a) low (0–1200 m a.s.l.), (b) mid (1200–2400 m a.s.l.), and (c) high bedrock altitudes (>2400 m a.s.l.). The x-axes show  
 relative time, from 0 (start of cooling phase with a temperature forcing of 0 K) to 1 (end of cooling phase with a temperature forcing of 0 K). At  
 0.5, half of the simulation is reached, where temperature forcing is strongest at  $-8$  K and the warming phase begins. In model years, the cooling  
 and warming phases span 2000 years each under fast and 4000 years each under slow temperature forcing. Therefore, the x-axes contain twice as  
 375 much absolute time for the slower compared to the faster temperature forcing.

## 4 Discussion

### 4.1 Resolution-related differences across bedrock altitude

Our results show that the ice field is generally thinner and faster-flowing at resolutions of 300 m and finer, in contrast to rather thick glaciers at resolutions coarser than 800 m, with strong changes at intermediate resolutions. We relate these differences between  
 380 fine and coarse resolution simulations to a combination of resampling effects in the input DEMs, glacier dynamics and feedback mechanisms. Generally, ice growth is supported by the coarse-resolution topography with flattened mountain peaks and gentle slopes, while fine resolutions accurately resolve topographic details which promotes ice flow speed-up and thinning in steeper and narrower valleys.

385 Despite the reduced high-altitude area, coarse-resolution DEMs with their gentle slopes (Fig. 1) tend to prevent glaciers from directly flowing into the ablation area, and thereby support ice thickening at high altitudes (Figs. 5, 7, 8). The shift from generally frozen bed conditions at fine resolution simulations to temperate basal ice at coarser resolutions is a consequence of different mechanisms, including colder climatic conditions in the fine resolution DEMs due to higher surface elevations. In contrast, the thicker ice at coarser resolutions is an effective insulator, trapping geothermal heat, while increased basal pressure lowers the pressure melting  
 390 point, increasing the possibility for basal melting.

In the valleys, ice flow at fine resolutions undergoes strong lateral confinement by steeper and narrower valley walls that forces the glaciers into a more constricted flow path. To satisfy mass conservation for ice as an incompressible fluid, this leads to accelerating ice flow and thus glacier thinning (Leger et al., 2025; Cuzzone et al., 2019). In contrast, at coarse resolutions, thicker ice flows more  
 395 slowly over smoother topography with gentler slopes (Fig. 7, 8). Among the finest resolutions, the reduction in ice velocity (Fig. 8) might result from increased lateral shear stress from very steep and narrow valley walls that impose resistance. In the valleys, the surface mass balance-elevation feedback plays an important role: When ice thickness increases, the ice surface reaches higher

elevations with lower temperatures, which promotes further ice growth (Levermann and Winkelmann, 2016). This feedback is most likely strongest in valleys with steep and narrow sidewalls at fine resolution and partly offsets ice thinning due to acceleration from channelized flow, indicated by consistently thicker ice at low altitudes than at high and mid altitudes - across all resolutions (Figs. 7, 8). At coarser resolutions, valley floors are elevated due to DEM resampling (Figs. 1, 2, 8), thereby expanding the accumulation zone and further enhancing ice build-up.

#### 4.2 Hysteresis effects

Our simulations show that the glaciers' response to changes in temperature are more accurately captured in the fine resolution simulations, where glaciers react more rapidly to transitions from cooling to warming periods (Figs. 3c, 9). Conversely, the delay in reaching maximum ice volume is exaggerated in coarser simulations and results are more affected by different temperature forcing rates. These hysteresis effects originate primarily from low-altitude regions (Fig. 4) and highlight the influence of the surface mass balance-elevation feedback, which allows valley glaciers to continue thickening despite rising temperatures. The thicker glaciers with underlying gentler slopes in the DEM at coarse resolution (Figs. 1, 8) result in generally shallower surface gradients (Fig. S6), thereby increasing the glacial response time compared to simulations at fine resolution (e.g., Cuffey and Paterson, 2010). For investigating more rapid climate change events in the geologic past or anthropogenic future with temperature variations of several degrees over centennial to millennial time scales, such as the Bølling-Allerød warming or the Younger Dryas cooling period (Rasmussen et al., 2006; Golledge et al., 2008; Norris et al., 2024; Patton et al., 2017), our results suggest that fine-resolution modelling is crucial to accurately capture the timing of glacial retreat and advances, while avoiding overestimated hysteresis effects.

#### 4.3 Topographic control on resolution-related differences in glacial modelling

Our results demonstrate that the accuracy of numerical models does not increase monotonically with spatial resolution. Similar to Williams et al. (2025) and Rückamp et al. (2020), we identify a spatial resolution that is sufficiently fine to produce results close to a fine-resolution reference run. However, in contrast to the km-scale resolution adequate for ice sheets in Greenland and Antarctica (Williams et al., 2025; Rückamp et al., 2020), we find that it requires a resolution of 300 m or finer to model the exemplary ice field in the topographically complex Western Alps. At such fine resolutions, the characteristic alpine topography is preserved with high accuracy (Figs. 1, 2, 8) and minor differences in elevation and slope effectively result in similar modelling results (Leger et al., 2025; Williams et al., 2025; Rückamp et al., 2020). However, the non-linear variations in model outputs at coarser resolutions cannot be explained exclusively by gradual changes in DEMs with resolution (Fig. 8 a, b). We argue that the interplay of topographic representation and ice dynamics causes these variations. For example, the ice build-up caused by raised valley floors at coarse resolutions is amplified by the surface mass balance-elevation feedback. We find that at ~800 m resolution, the topographic constraints become sufficiently weakened so that further coarsening has a minor additional effect. At these resolutions, glacier geometry is increasingly controlled by surface elevation in terms of ice thickness rather than bedrock relief, which is enhanced by the surface mass balance-elevation feedback. At intermediate resolutions of 400–800 m, continuous and large changes with resolution mark the transition between the topographically- and thickness-controlled ice dynamics.

Additional experiments with smoothed topographies that are on average  $10^\circ$  less steep than the present-day Alps and mean slopes similar to mountain ranges like, e.g., the Scottish Highlands (e.g., Whitbread et al., 2015) show that spatial resolution has a similar influence on ice dynamics which is again dependent on bedrock altitudes (Figs. S8, S9). In these experiments, we observe strong variations between ~500–700 m resolution (Fig. S9) and comparable results at resolutions of 400 m and finer, which are only slightly coarser compared to simulations using the original DEM. This emphasizes the importance of running simulations at resolutions at least finer than km- and ideally 400-m-scale, even in relatively smooth mountainous terrain. We expect similar resolution-dependent

patterns at high, mid and low altitudes in other mountainous regions, where specific altitude bands may shift depending on regional topographic features.

440 To overcome resolution-dependent errors in ice modelling, it is necessary to identify a sufficiently fine resolution to model a topographically controlled rather than a too smooth and thick ice field. However, even seemingly stable results at coarse resolutions (900–2000 m) do not indicate that the chosen resolution is sufficient, because model outputs show large variations at intermediate resolutions (400–800 m). A series of tests and considerations of spatial difference patterns might help to detect a sufficiently fine resolution and ensure that an even finer resolution does not substantially influence the ice dynamics. Specifically, checking if  
445 surfaces of glacier flowing over mountain summits are realistically represented might be an initial indicator, as models at coarse resolutions might show imprints of bedrock topography onto the ice surface (Fig. 6). Similar features can be observed in simulations of glaciations in the European Alps at 1–2 km resolution using PISM (Fig. 5 in Leger et al., 2025; supplementary data in Jouvét et al., 2023 and Seguinot et al., 2018), implying that these artefacts are not related to IGM. In such coarse resolution DEMs, strong variations in surface gradients between neighbouring grid cells are problematic in spatially discretized models based on finite  
450 differences or elements schemes. In contrast, although slopes are steeper at fine resolutions, valleys and mountains are represented across several cells, improving numerical stability. Testing for such artifacts only requires small subsets, and therefore limited computational resources. Without thorough consideration of resolution, however, the model parameters may be tuned to produce seemingly accurate glacier geometries that, in fact, compensate for unrealistic terrain representations in too coarse DEMs.

#### 4.4 Limitations of the employed modelling

455 At fine resolutions that are required to accurately model ice field dynamics, the Blatter-Pattyn approximation implemented in IGM may deviate from the full Stokes solution and exhibit mechanical inaccuracies, particularly in steep terrain (Rückamp et al., 2022; Yan et al., 2023; Hindmarsh, 2004). The presented study deliberately focuses on numerical rather than mechanical errors and demonstrated that substantial numerical errors already occur at spatial resolutions commonly used in large-scale mountain ice-cover simulations (e.g., Mey et al., 2016; Seguinot et al., 2018; Jouvét et al., 2023; Golledge et al., 2012; Zhang et al., 2022). Deviations  
460 between modelled velocities in a Greenland ice stream region using the Blatter-Pattyn compared to a full Stokes model are less than  $\sim 10 \text{ m yr}^{-1}$ , as investigated by Rückamp et al. (2022), and therefore smaller than the resolution-induced differences of up to several tens of meters per year found in our analysis. Therefore, adopting a full Stokes formulation would substantially increase computational costs without addressing the main source of error. Future studies are needed to systematically assess the benefits of full Stokes models at fine resolutions in alpine regions.

465 For practical considerations, we argue that improving numerical accuracy through finer spatial resolution is a necessary prerequisite before resorting to mechanically more sophisticated ice-flow models. Additional model components such as incorporating erosion processes, potentially enhance resolution-related effects by altering valley shapes (Liebl et al., 2021; Valla et al., 2011). The accelerated ice flow in fine-resolution models is expected to enhance the carving of larger trunk valleys, whereas thin and bed-  
470 frozen ice-covers shield high altitude plateaus from erosion processes, and ice-free parts are exposed to non-glacial erosion (Bernard et al., 2025; Egholm et al., 2017). Continued model development is essential to allow for higher-resolution modelling over large time and spatial scales at reasonable computational costs, for example through GPU-based approaches.

## 5 Conclusions

To assess the impact of spatial resolution on model outputs, we simulated the hypothetical growth and decline of a large mountainous ice field in the European Alps over multi-millennial time scales at different resolutions ranging from 50 m to 2 km. The simulations over both, large spatial scale and several millennia were made possible by the GPU-based architecture of the Instructed Glacier Model (IGM). Although total glaciated areas are similar across all resolutions, differences in ice thickness and thus volume are substantial, with high variations between resolutions of 300 m and 800 m. These differences are unequally distributed across the terrain. At high altitudes, coarse resolutions result in flatter mountain tops and shallower slopes that provide a larger accumulation area and thus thicker and slower flowing ice. At maximum glaciation, the ice is typically warm-based at coarse resolutions, while the thinner glaciers on steeper and higher mountains in fine-resolution runs remain cold-based. Elevated valley floors in the coarse-resolution runs enhance ice thickness increase via the surface mass balance-elevation feedback. Large and deeply incised valleys at low altitudes are less affected by resampling to a coarser resolution but their glaciers thicken substantially, while ice flow at fine resolutions is accelerated, resulting in generally thinner valley glaciers. Glacial response time is also affected by spatial resolution, with thicker glaciers at coarse resolutions responding more slowly to temperature changes and exhibiting stronger hysteresis effects. This behaviour depends on the rate of temperature change but persists for the tested cooling and warming rates of 2 and 4 K/kyr.

We conclude that for a mountain range like the European Alps, a resolution of 300 m or finer is sufficient to resolve bedrock slopes, resulting in a more topographically constrained ice field. Seemingly stable model outputs at coarse resolution may be misleading and arise from ice dynamics driven by inaccurately resolved topography. Experiments using a smoothed DEM suggest that the non-linear, altitudinal-dependent influence of spatial resolution are also expected across other mountain regions that are less steep than the European Alps.

## 6 Code and data availability

The Instructed Glacier Model (IGM) source code (Python programming language) and documentation are available from Guillaume Jouvét's GitHub repository at <https://github.com/jouvetg/igm>. We used IGM version 2.2.1 and commit 19bf4151d77f97841aacd8d0b743096e48863970. The IGM model setup from Leger et al. (2025) used in this study is accessible via <https://zenodo.org/records/14275231>.

## 7 Author contributions

Conceptualization: HW, DS, support from TPML, GJ. Methodology: HW, DS, TPML, GJ. Investigation: HW, support from DS. Visualization: HW, support from DS and TPML. Supervision: DS, support from RW. Writing (original draft): HW, support from DS. Writing (review and editing): HW, DS, TPML, GJ, RW.

## 8 Competing interests

The authors declare that they have no conflict of interest.

## 9 Acknowledgements

This study was supported by the German Research Foundation (DFG) grant to Dirk Scherler (SCHE 1676/6-1) and Ricarda Winkelmann under the priority program "Mountain Building Processes in Four Dimensions (MB-4D)" and by the European

Research Council under the European Union's Horizon 2020 research and innovation programme under grant agreement 759639. This work utilized high-performance computing resources made possible by funding from the Ministry of Science, Research and Culture of the State of Brandenburg (MWFK) and are operated by the IT Services and Operations unit of the Helmholtz Centre  
510 Potsdam.

## 10 References

Aschwanden, A., Bueler, E., Khroulev, C., and Blatter, H.: An enthalpy formulation for glaciers and ice sheets, *J. Glaciol.*, 58, 441–457, <https://doi.org/10.3189/2012JoG11J088>, 2012.

515 Aschwanden, A., Fahnestock, M. A., and Truffer, M.: Complex Greenland outlet glacier flow captured, *Nat Commun*, 7, 10524, <https://doi.org/10.1038/ncomms10524>, 2016.

Bernard, M., Van Der Beek, P. A., Pedersen, V. K., and Colleps, C.: Production and Preservation of Elevated Low-Relief Surfaces in Mountainous Landscapes by Pliocene-Quaternary Glaciations, *AGU Advances*, 6, e2024AV001610, <https://doi.org/10.1029/2024AV001610>, 2025.

520 Blatter, H.: Velocity and stress fields in grounded glaciers: a simple algorithm for including deviatoric stress gradients, *J. Glaciol.*, 41, 333–344, <https://doi.org/10.3189/S002214300001621X>, 1995.

Calov, R. and Greve, R.: A semi-analytical solution for the positive degree-day model with stochastic temperature variations, *J. Glaciol.*, 51, 173–175, <https://doi.org/10.3189/172756505781829601>, 2005.

525 Cook, S. J., Jouvét, G., Millan, R., Rabatel, A., Zekollari, H., and Dussaillant, I.: Committed Ice Loss in the European Alps Until 2050 Using a Deep-Learning-Aided 3D Ice-Flow Model With Data Assimilation, *Geophysical Research Letters*, 50, e2023GL105029, <https://doi.org/10.1029/2023GL105029>, 2023.

Cuffey, K. and Paterson, W. S. B.: *The physics of glaciers*, 4th ed., Butterworth-Heinemann/Elsevier, Burlington, MA, 693 pp., 2010.

530 Cuzzone, J. K., Schlegel, N.-J., Morlighem, M., Larour, E., Briner, J. P., Seroussi, H., and Caron, L.: The impact of model resolution on the simulated Holocene retreat of the southwestern Greenland ice sheet using the Ice Sheet System Model (ISSM), *The Cryosphere*, 13, 879–893, <https://doi.org/10.5194/tc-13-879-2019>, 2019.

Duncan, C., Masek, J., and Fielding, E.: How steep are the Himalaya? Characteristics and implications of along-strike topographic variations, *Geol*, 31, 75, [https://doi.org/10.1130/0091-7613\(2003\)031<0075:HSATHC>2.0.CO;2](https://doi.org/10.1130/0091-7613(2003)031<0075:HSATHC>2.0.CO;2), 2003.

535 Egholm, D. L., Jansen, J. D., Brødstrup, C. F., Pedersen, V. K., Andersen, J. L., Ugelvig, S. V., Larsen, N. K., and Knudsen, M. F.: Formation of plateau landscapes on glaciated continental margins, *Nature Geosci*, 10, 592–597, <https://doi.org/10.1038/ngeo2980>, 2017.

Gagliardini, O., Zwinger, T., Gillet-Chaulet, F., Durand, G., Favier, L., De Fleurian, B., Greve, R., Malinen, M., Martín, C., Råback, P., Ruokolainen, J., Sacchetti, M., Schäfer, M., Seddik, H., and Thies, J.: Capabilities and performance of Elmer/Ice, a new-generation ice sheet model, *Geosci. Model Dev.*, 6, 1299–1318, <https://doi.org/10.5194/gmd-6-1299-2013>, 2013.

540 Golledge, N. R., Hubbard, A., and Sugden, D. E.: High-resolution numerical simulation of Younger Dryas glaciation in Scotland, *Quaternary Science Reviews*, 27, 888–904, <https://doi.org/10.1016/j.quascirev.2008.01.019>, 2008.

Golledge, N. R., Mackintosh, A. N., Anderson, B. M., Buckley, K. M., Doughty, A. M., Barrell, D. J. A., Denton, G. H., Vandergoes, M. J., Andersen, B. G., and Schaefer, J. M.: Last Glacial Maximum climate in New Zealand inferred from a modelled Southern Alps icefield, *Quaternary Science Reviews*, 46, 30–45, <https://doi.org/10.1016/j.quascirev.2012.05.004>, 2012.

545 Goutorbe, B., Poort, J., Lucazeau, F., and Raillard, S.: Global heat flow trends resolved from multiple geological and geophysical proxies, *Geophysical Journal International*, 187, 1405–1419, <https://doi.org/10.1111/j.1365-246X.2011.05228.x>, 2011.

Hartmeyer, I., Delleske, R., Keuschnig, M., Krautblatter, M., Lang, A., Schrott, L., and Otto, J.-C.: Current glacier recession causes significant rockfall increase: the immediate paraglacial response of deglaciating cirque walls, *Earth Surf. Dynam.*, 8, 729–751, <https://doi.org/10.5194/esurf-8-729-2020>, 2020.

- Hindmarsh, R. C. A.: A numerical comparison of approximations to the Stokes equations used in ice sheet and glacier modeling, *Journal of Geophysical Research: Earth Surface*, 109, <https://doi.org/10.1029/2003JF000065>, 2004.
- 550 Hock, R.: Temperature index melt modelling in mountain areas, *Journal of Hydrology*, 282, 104–115, [https://doi.org/10.1016/S0022-1694\(03\)00257-9](https://doi.org/10.1016/S0022-1694(03)00257-9), 2003.
- Huggel, C., Muccione, V., Carey, M., James, R., Jurt, C., and Mechler, R.: Loss and Damage in the mountain cryosphere, *Reg Environ Change*, 19, 1387–1399, <https://doi.org/10.1007/s10113-018-1385-8>, 2019.
- 555 Hugonnet, R., McNabb, R., Berthier, E., Menounos, B., Nuth, C., Girod, L., Farinotti, D., Huss, M., Dussailant, I., Brun, F., and Kääh, A.: Accelerated global glacier mass loss in the early twenty-first century, *Nature*, 592, 726–731, <https://doi.org/10.1038/s41586-021-03436-z>, 2021.
- Immerzeel, W. W., Lutz, A. F., Andrade, M., Bahl, A., Biemans, H., Bolch, T., Hyde, S., Brumby, S., Davies, B. J., Elmore, A. C., Emmer, A., Feng, M., Fernández, A., Haritashya, U., Kargel, J. S., Koppes, M., Kraaijenbrink, P. D. A., Kulkarni, A. V., Mayewski, P. A., Nepal, S., Pacheco, P., Painter, T. H., Pellicciotti, F., Rajaram, H., Rupper, S., Sinisalo, A., Shrestha, A. B., Viviroli, D., Wada, Y., Xiao, C., Yao, T., and Baillie, J. E. M.: Importance and vulnerability of the world’s water towers, *Nature*, 577, 364–369, <https://doi.org/10.1038/s41586-019-1822-y>, 2020.
- 560 Isotta, F. A., Frei, C., Weigluni, V., Perčec Tadić, M., Lassègues, P., Rudolf, B., Pavan, V., Cacciamani, C., Antolini, G., Ratto, S. M., Munari, M., Micheletti, S., Bonati, V., Lussana, C., Ronchi, C., Panettieri, E., Marigo, G., and Vertačnik, G.: The climate of daily precipitation in the Alps: development and analysis of a high-resolution grid dataset from pan-Alpine rain-gauge data, *International Journal of Climatology*, 34, 1657–1675, <https://doi.org/10.1002/joc.3794>, 2014.
- 565 Ivy-Ochs, S.: Glacier variations in the European Alps at the end of the last glaciation, *CIG*, 41, 295–315, <https://doi.org/10.18172/cig.2750>, 2015.
- Jouvet, G. and Cordonnier, G.: Ice-flow model emulator based on physics-informed deep learning, *J. Glaciol.*, 69, 1941–1955, <https://doi.org/10.1017/jog.2023.73>, 2023.
- 570 Jouvet, G., Cohen, D., Russo, E., Buzan, J., Raible, C. C., Haeberli, W., Kamleitner, S., Ivy-Ochs, S., Imhof, M. A., Becker, J. K., Landgraf, A., and Fischer, U. H.: Coupled climate-glacier modelling of the last glaciation in the Alps, *J. Glaciol.*, 69, 1956–1970, <https://doi.org/10.1017/jog.2023.74>, 2023.
- Jouzel, J. and Masson-Delmotte, V.: EPICA Dome C Ice Core 800KYr deuterium data and temperature estimates, <https://doi.org/10.1594/PANGAEA.683655>, 2007.
- 575 Kamleitner, S., Ivy-Ochs, S., Monegato, G., Gianotti, F., Akçar, N., Vockenhuber, C., Christl, M., and Synal, H.-A.: The Ticino-Toce glacier system (Swiss-Italian Alps) in the framework of the Alpine Last Glacial Maximum, *Quaternary Science Reviews*, 279, 107400, <https://doi.org/10.1016/j.quascirev.2022.107400>, 2022.
- Kessler, M. A., Anderson, R. S., and Stock, G. M.: Modeling topographic and climatic control of east-west asymmetry in Sierra Nevada glacier length during the Last Glacial Maximum, *J. Geophys. Res.*, 111, 2005JF000365, <https://doi.org/10.1029/2005JF000365>, 2006.
- 580 Korup, O., Schmidt, J., and McSaveney, M. J.: Regional relief characteristics and denudation pattern of the western Southern Alps, New Zealand, *Geomorphology*, 71, 402–423, <https://doi.org/10.1016/j.geomorph.2005.04.013>, 2005.
- Leger, T. P. M., Jouvet, G., Kamleitner, S., Mey, J., Herman, F., Finley, B. D., Ivy-Ochs, S., Vieli, A., Henz, A., and Nussbaumer, S. U.: A data-consistent model of the last glaciation in the Alps achieved with physics-driven AI, *Nat Commun*, 16, 848, <https://doi.org/10.1038/s41467-025-56168-3>, 2025.
- 585 Levermann, A. and Winkelmann, R.: A simple equation for the melt elevation feedback of ice sheets, *The Cryosphere*, 10, 1799–1807, <https://doi.org/10.5194/tc-10-1799-2016>, 2016.
- Liebl, M., Robl, J., Egholm, D. L., Prasicek, G., Stüwe, K., Gradwohl, G., and Hergarten, S.: Topographic signatures of progressive glacial landscape transformation, *Earth Surf Processes Landf*, 46, 1964–1980, <https://doi.org/10.1002/esp.5139>, 2021.
- 590 Meier, W. J.-H., Grieflinger, J., Hochreuther, P., and Braun, M. H.: An Updated Multi-Temporal Glacier Inventory for the Patagonian Andes With Changes Between the Little Ice Age and 2016, *Front. Earth Sci.*, 6, 62, <https://doi.org/10.3389/feart.2018.00062>, 2018.

- Fiche climatologique. Statistiques 1981-2010 et records:  
 595 [https://donneespubliques.meteofrance.fr/FichesClim/FICHECLIM\\_73157002.pdf](https://donneespubliques.meteofrance.fr/FichesClim/FICHECLIM_73157002.pdf), last access: 28 November 2025.
- Mey, J., Scherler, D., Wickert, A. D., Egholm, D. L., Tesauro, M., Schildgen, T. F., and Strecker, M. R.: Glacial isostatic uplift of the European Alps, *Nat Commun*, 7, 13382, <https://doi.org/10.1038/ncomms13382>, 2016.
- Millan, R., Mouginot, J., Rabatel, A., and Morlighem, M.: Ice velocity and thickness of the world's glaciers, *Nat. Geosci.*, 15, 124–129, <https://doi.org/10.1038/s41561-021-00885-z>, 2022.
- 600 Minh, N. Q., Huong, N. T. T., Khanh, P. Q., Hien, L. P., and Bui, D. T.: Impacts of Resampling and Downscaling Digital Elevation Model and Its Morphometric Factors: A Comparison of Hopfield Neural Network, Bilinear, Bicubic, and Kriging Interpolations, *Remote Sensing*, 16, 819, <https://doi.org/10.3390/rs16050819>, 2024.
- Norris, S. L., Margold, M., Evans, D. J. A., Atkinson, N., and Froese, D. G.: Dynamical response of the southwestern Laurentide Ice Sheet to rapid Bølling–Allerød warming, *The Cryosphere*, 18, 1533–1559, <https://doi.org/10.5194/tc-18-1533-2024>, 2024.
- 605 Nowicki, S. M. J., Payne, A., Larour, E., Seroussi, H., Goelzer, H., Lipscomb, W., Gregory, J., Abe-Ouchi, A., and Shepherd, A.: Ice Sheet Model Intercomparison Project (ISMIP6) contribution to CMIP6, *Geosci. Model Dev.*, 9, 4521–4545, <https://doi.org/10.5194/gmd-9-4521-2016>, 2016.
- Patton, H., Hubbard, A., Andreassen, K., Auriac, A., Whitehouse, P. L., Stroeven, A. P., Shackleton, C., Winsborrow, M., Heyman, J., and Hall, A. M.: Deglaciation of the Eurasian ice sheet complex, *Quaternary Science Reviews*, 169, 148–172,  
 610 <https://doi.org/10.1016/j.quascirev.2017.05.019>, 2017.
- Pattyn, F., Perichon, L., Aschwanden, A., Breuer, B., de Smedt, B., Gagliardini, O., Gudmundsson, G. H., Hindmarsh, R. C. A., Hubbard, A., Johnson, J. V., Kleiner, T., Konovalov, Y., Martin, C., Payne, A. J., Pollard, D., and Price, S.: Benchmark experiments for higher-order and full-Stokes ice sheet models (ISMIP–HOM), *The Cryosphere*, 2008.
- Penck, A. and Brückner, E.: *Die Alpen im Eiszeitalter*, Tauchnitz, 540 pp., 1909.
- 615 Rasmussen, S. O., Andersen, K. K., Svensson, A. M., Steffensen, J. P., Vinther, B. M., Clausen, H. B., Siggaard-Andersen, M. -L., Johnsen, S. J., Larsen, L. B., Dahl-Jensen, D., Bigler, M., Röthlisberger, R., Fischer, H., Goto-Azuma, K., Hansson, M. E., and Ruth, U.: A new Greenland ice core chronology for the last glacial termination, *J. Geophys. Res.*, 111, 2005JD006079, <https://doi.org/10.1029/2005JD006079>, 2006.
- Rückamp, M., Goelzer, H., and Humbert, A.: Sensitivity of Greenland ice sheet projections to spatial resolution in higher-order simulations: the Alfred Wegener Institute (AWI) contribution to ISMIP6 Greenland using the Ice-sheet and Sea-level System Model (ISSM), *The Cryosphere*, 14, 3309–3327, <https://doi.org/10.5194/tc-14-3309-2020>, 2020.
- 620 Rückamp, M., Kleiner, T., and Humbert, A.: Comparison of ice dynamics using full-Stokes and Blatter–Pattyn approximation: application to the Northeast Greenland Ice Stream, *The Cryosphere*, 16, 1675–1696, <https://doi.org/10.5194/tc-16-1675-2022>, 2022.
- Schoof, C. and Hewitt, I.: Ice-Sheet Dynamics, *Annu. Rev. Fluid Mech.*, 45, 217–239, <https://doi.org/10.1146/annurev-fluid-011212-140632>, 2013.
- 625 Seguinot, J., Ivy-Ochs, S., Jouvét, G., Huss, M., Funk, M., and Preusser, F.: Modelling last glacial cycle ice dynamics in the Alps, *The Cryosphere*, 12, 3265–3285, <https://doi.org/10.5194/tc-12-3265-2018>, 2018.
- Strahler, A. N.: Quantitative analysis of watershed geomorphology, *Eos Trans. AGU*, 38, 913–920, <https://doi.org/10.1029/TR038i006p00913>, 1957.
- 630 Tadono, T., Ishida, H., Oda, F., Naito, S., Minakawa, K., and Iwamoto, H.: Precise Global DEM Generation by ALOS PRISM, *ISPRS Ann. Photogramm. Remote Sens. Spatial Inf. Sci.*, II–4, 71–76, <https://doi.org/10.5194/isprsannals-II-4-71-2014>, 2014.
- Valla, P. G., Shuster, D. L., and Van Der Beek, P. A.: Significant increase in relief of the European Alps during mid-Pleistocene glaciations, *Nature Geosci*, 4, 688–692, <https://doi.org/10.1038/ngeo1242>, 2011.
- 635 Whitbread, K., Jansen, J., Bishop, P., and Attal, M.: Substrate, sediment, and slope controls on bedrock channel geometry in postglacial streams, *JGR Earth Surface*, 120, 779–798, <https://doi.org/10.1002/2014JF003295>, 2015.

Wickert, A. D.: Open-source modular solutions for flexural isostasy: gFlex v1.0, <https://doi.org/10.5194/gmdd-8-4245-2015>, 2 June 2015.

Williams, C. R., Thodoroff, P., Arthern, R. J., Byrne, J., Hosking, J. S., Kaiser, M., Lawrence, N. D., and Kazlauskaitė, I.: Calculations of extreme sea level rise scenarios are strongly dependent on ice sheet model resolution, *Commun Earth Environ*, 6, 60, <https://doi.org/10.1038/s43247-025-02010-z>, 2025.

Winkelmann, R., Martin, M. A., Haseloff, M., Albrecht, T., Bueller, E., Khroulev, C., and Levermann, A.: The Potsdam Parallel Ice Sheet Model (PISM-PIK) – Part 1: Model description, *The Cryosphere*, 5, 715–726, <https://doi.org/10.5194/tc-5-715-2011>, 2011.

Wirsig, C., Zasadni, J., Christl, M., Akçar, N., and Ivy-Ochs, S.: Dating the onset of LGM ice surface lowering in the High Alps, *Quaternary Science Reviews*, 143, 37–50, <https://doi.org/10.1016/j.quascirev.2016.05.001>, 2016.

645 Yan, Z., Leng, W., Wang, Y., Xiao, C., and Zhang, T.: A comparison between three-dimensional, transient, thermomechanically coupled first-order and Stokes ice flow models, *Journal of Glaciology*, 69, 513–524, <https://doi.org/10.1017/jog.2022.77>, 2023.

Zhang, R., Zhang, Z., Jiang, D., Ramstein, G., Dupont-Nivet, G., and Li, X.: Tibetan Plateau Made Central Asian Drylands Move Northward, Concentrate in Narrow Latitudinal Bands, and Increase in Intensity During the Cenozoic, *Geophysical Research Letters*, 49, e2021GL093718, <https://doi.org/10.1029/2021GL093718>, 2022.

650